

SUPPORTING INFORMATION

Bulk passivation and suppressing nonradiative recombination loss in 3D all-inorganic CsPbIBr₂ perovskite solar cell via 2D layered perovskite framework

Tapas Das¹, Faisal Farooq², Parul Garg², Sakal Singla², Asim Guchhait^{1*}, Ashok Bera^{2*}

¹Department of Physics, Prabhat Kumar College, Karkuli, Contai, West Bengal, India, 721 404

²Department of Physics, Indian Institute of Technology Jammu, J & K 181221, India.

[*guchhait.asim@gmail.com](mailto:guchhait.asim@gmail.com)

[*ashok.bera@iitjammu.ac.in](mailto:ashok.bera@iitjammu.ac.in)

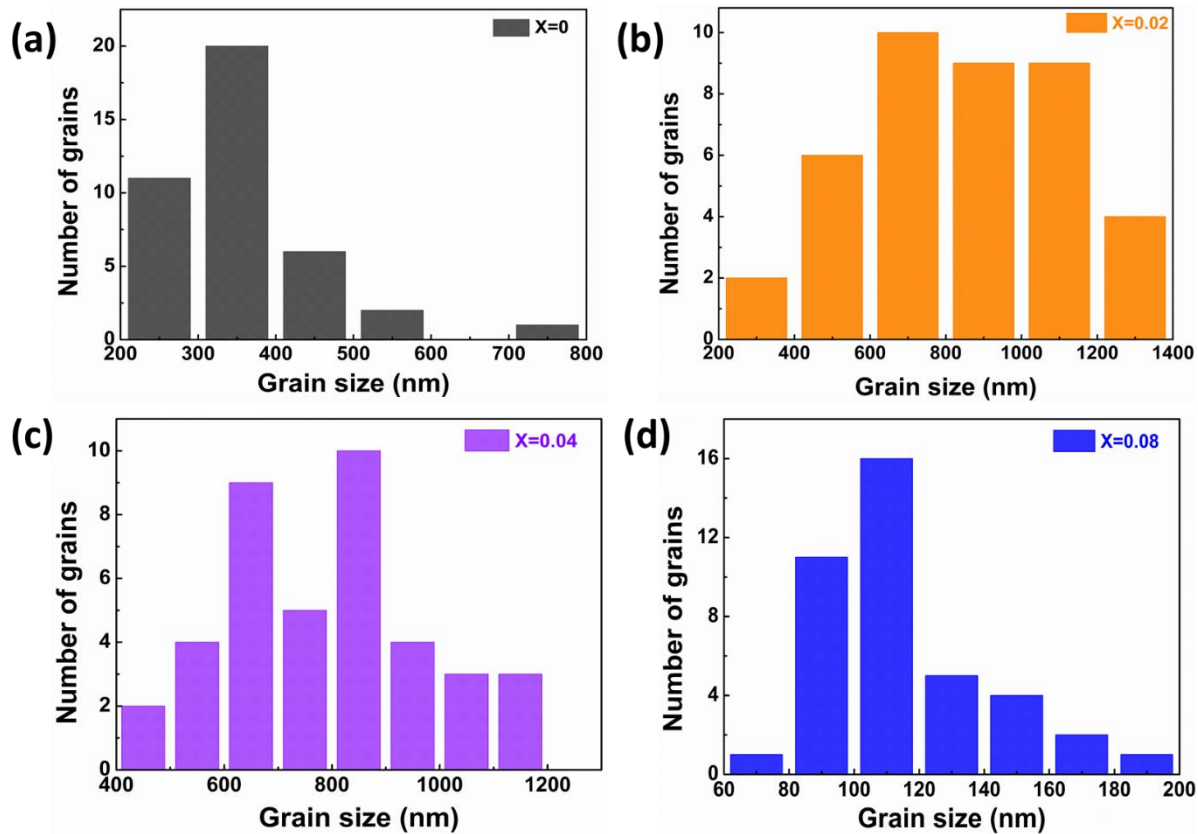


Fig. S1. Histogram analyses of the grain size distribution of the (a) $X=0$, (b) $X=0.02$, (c) $X=0.04$, (d) $X=0.08$ perovskite thin films deposited on bare glass substrates.

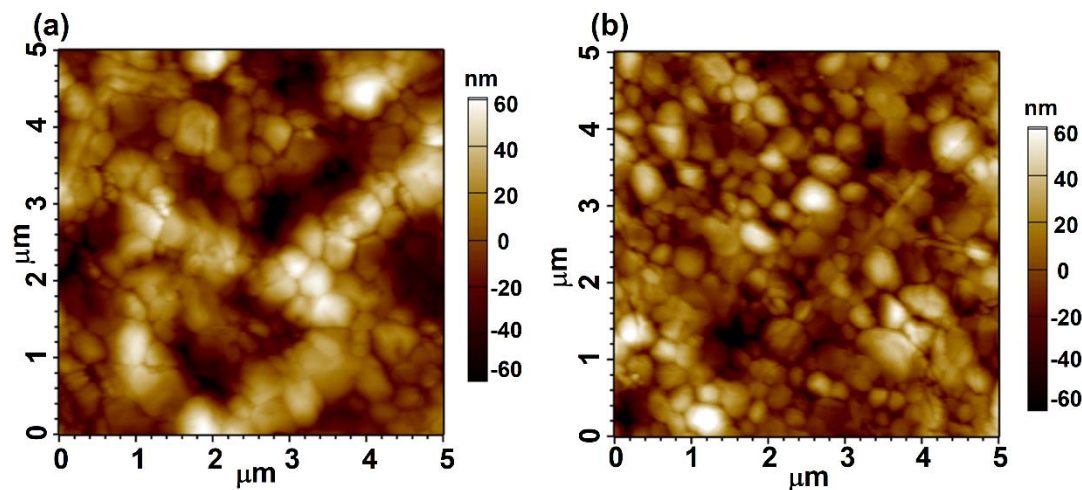


Fig. S2. Top-surface AFM image of (a) pristine CsPbIBr_2 and (b) PEAI doped CsPbIBr_2 thin film.

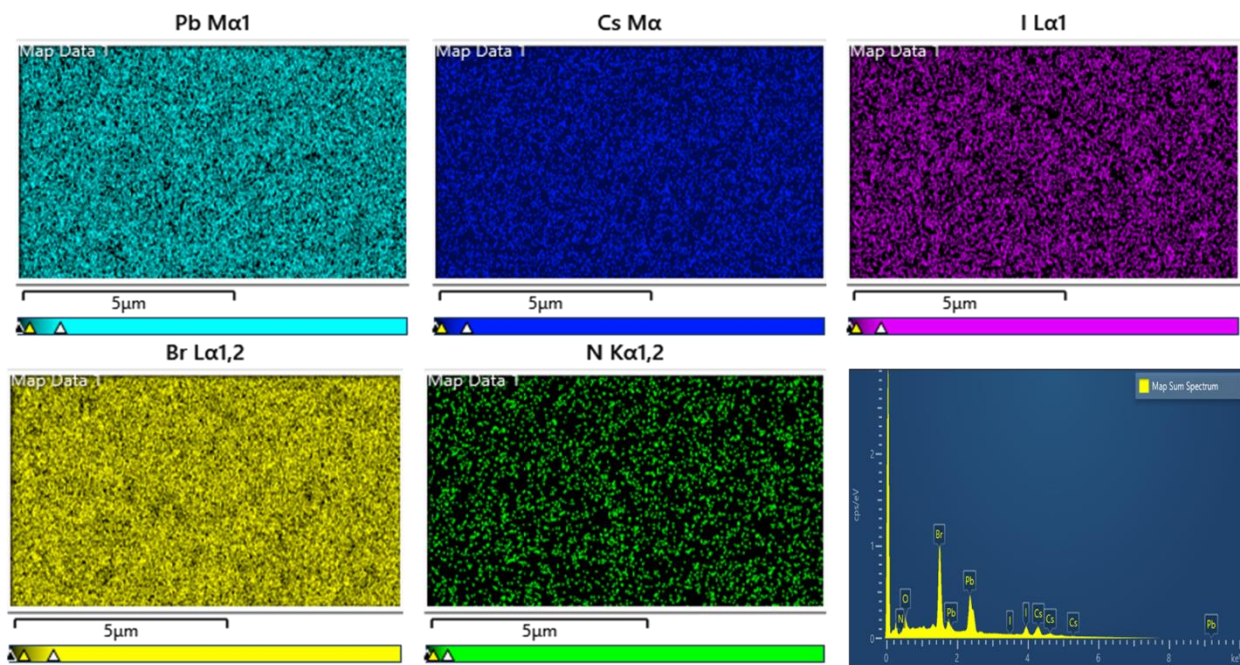


Fig. S3. Elemental mapping with the map sum spectrum (bottom right one) of the synthesized $((\text{PEA})_2\text{PbI}_4)_{0.02}(\text{CsPbIBr}_2)_{0.98}$ perovskite thin film on a bare glass substrate.

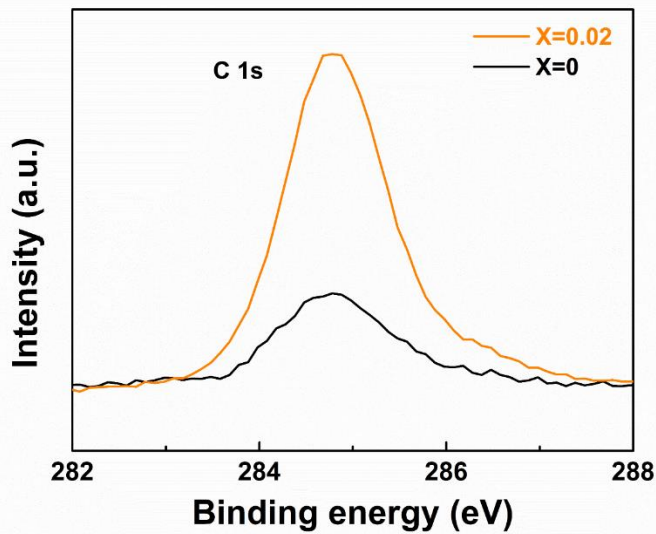


Fig. S4. High-resolution XPS spectrum corresponding to the analyses of C1s peak.

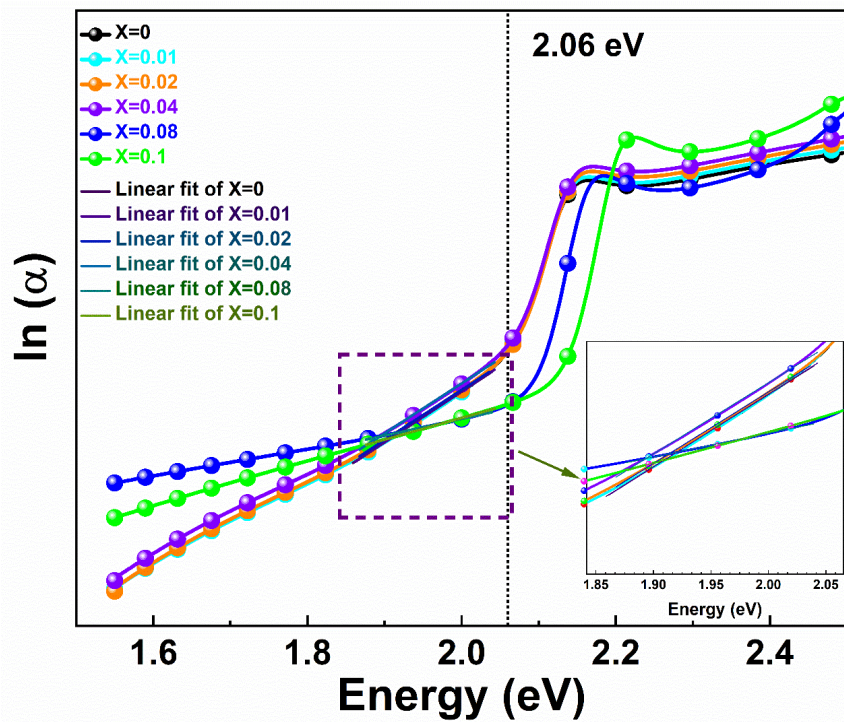


Fig. S5. Urbach energy analysis from the light absorbance spectrum of the fabricated $((\text{PEA})_2\text{PbI}_4)_X(\text{CsPbIBr}_2)_{1-X}$ perovskite thin films deposited on bare glass substrates.

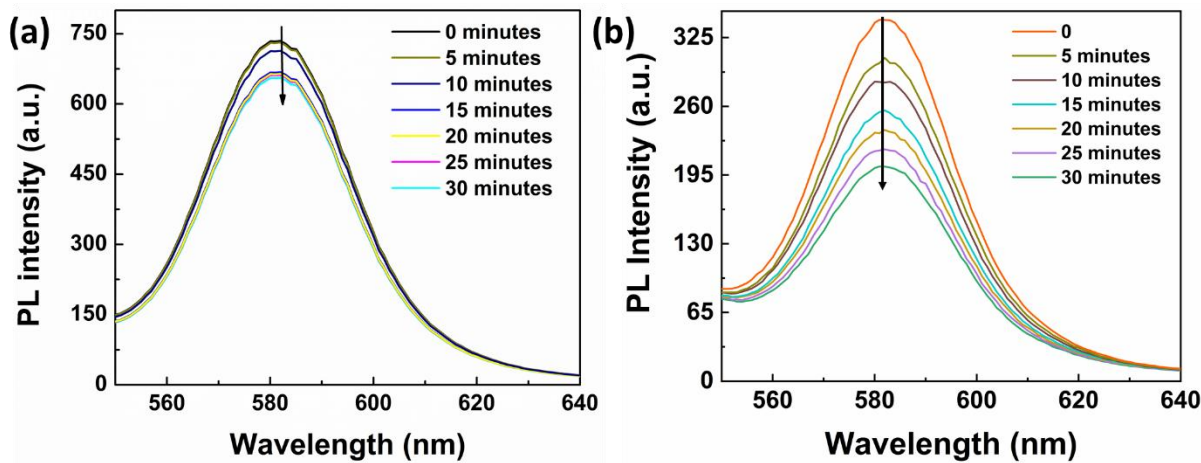


Fig. S6. PL degradation test of the fabricated (a) $X=0.02$, and (b) $X=0$ based perovskite thin films under the ambient environment ($RT \approx 27^\circ\text{C}$, $RH \approx 84\%$) for initial 30 minutes.

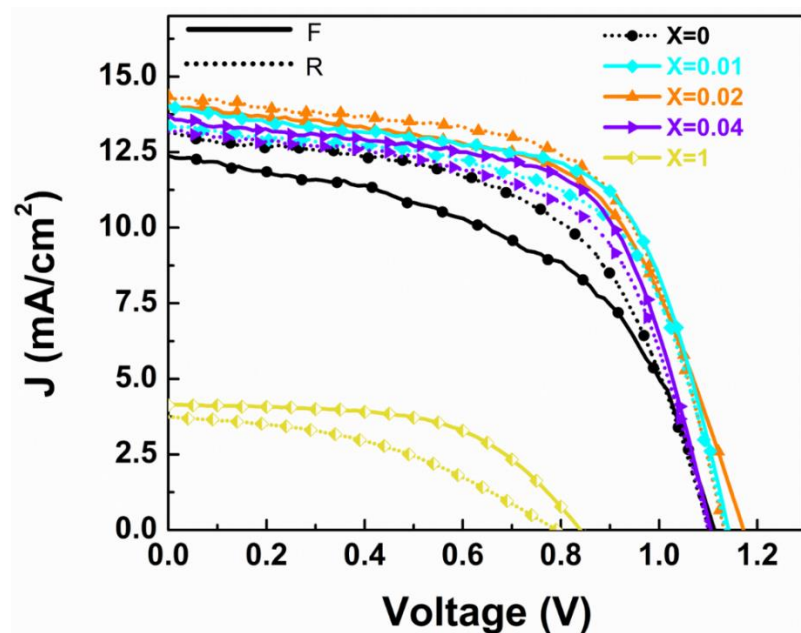


Fig. S7. Light-illuminated J - V analyses of the fabricated PSCs using the $((\text{PEA})_2\text{PbI}_4)_X(\text{CsPbIBr}_2)_{1-X}$ perovskite absorber layer where $X=0, 0.01, 0.02, 0.04, 1$.

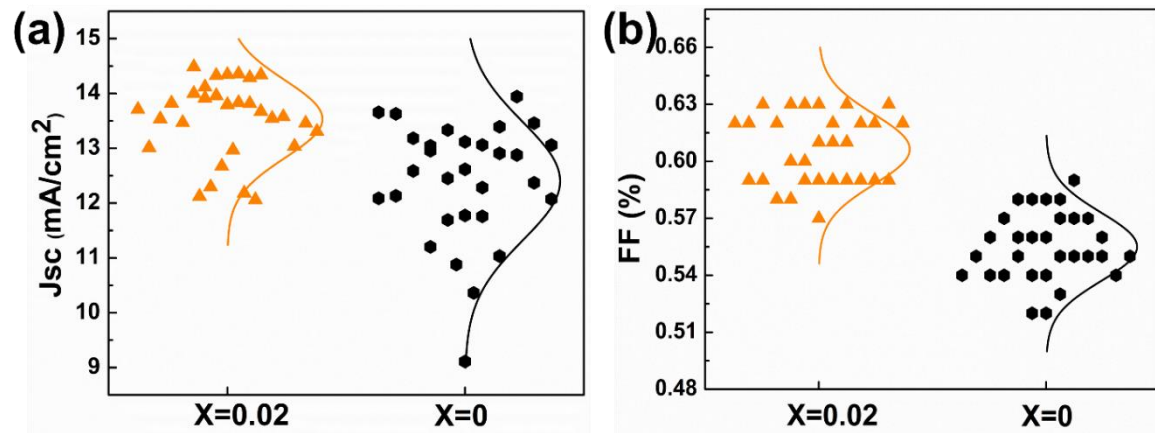


Fig. S8. Device repeatability concerning to the (a) J_{SC} , and (b) FF .

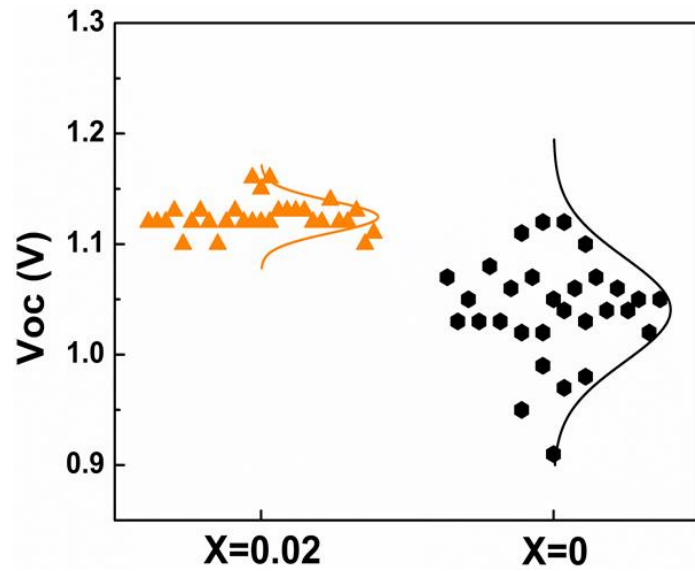


Fig. S9. Device repeatability concerning to the V_{OC} .

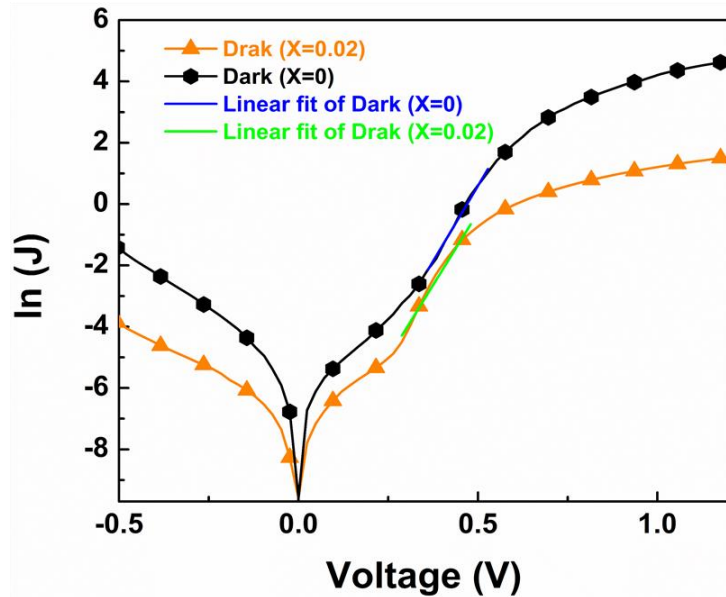


Fig. S10. Semi-log dark J-V plot of the fabricated pristine, and champion devices.

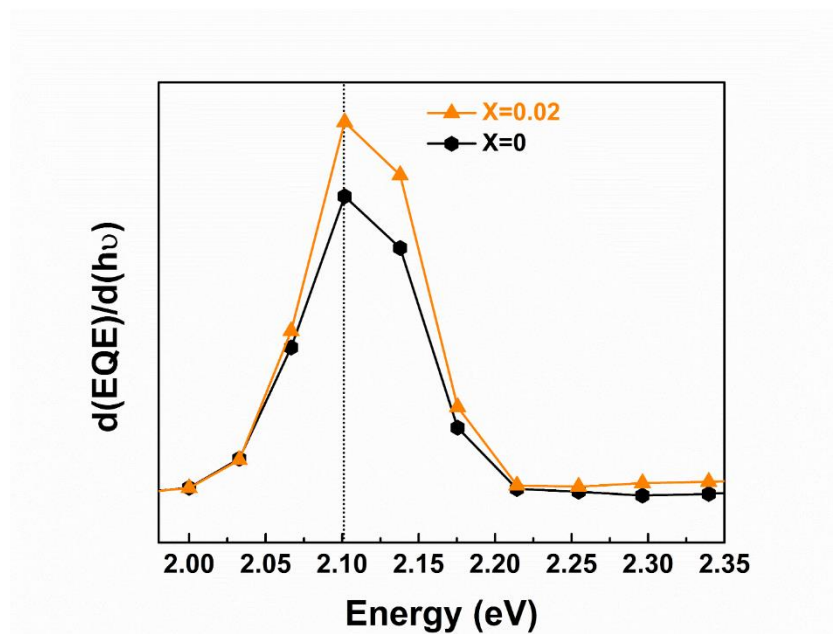


Fig. S11. Bandgap calculation from the EQE plot of the fabricated pristine, and champion devices.

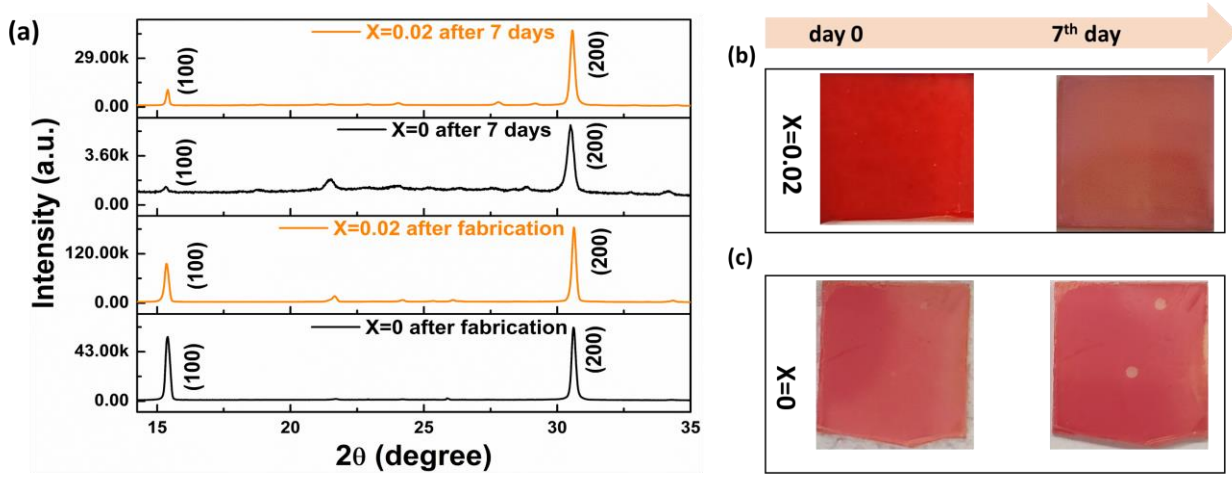


Fig. S12. (a) XRD pattern of the fabricated perovskite thin films ($X=0$, 0.02) stored under an ambient environment ($\text{RH} \approx 60\%$, RT 26°C) for 7 days, and real-time digital photographs of the fabricated perovskite thin films having (b) $X=0.02$, & (c) $X=0$.

Table S1. Calculated crystal structure parameters of the (200) crystal plane from the XRD pattern of the fabricated perovskite thin films.

Perovskite thin films with 2D ratio	Position of the crystallite plane (degree)	FWHM (degree)	Crystallite size (nm)	Inter planer distance (nm)	Lattice parameter (nm)
$X=0$	30.60	0.1833	44.931	0.2919	0.5838
$X=0.02$	30.62	0.1826	53.599	0.2917	0.5834
$X=0.04$	30.63	0.1837	44.838	0.2916	0.5832
$X=0.08$	30.37	0.2086	39.460	0.2940	0.5880

Table S2. Statistical analyses of 40 grains of the fabricated $((\text{PEA})_2\text{PbI}_4)_x(\text{CsPbIBr}_2)_{1-x}$ perovskite thin films spin-coated on bare glass substrates.

Samples	Average grain size with standard deviation
X=0	350.43±0.09 709 nm
X=0.02	853.38±0.18 1367 nm
X=0.04	795.78±0.23 1109 nm
X=0.08	114.28±0.56 181.64 nm

- The bolded grain sizes are the maximum of the 30 grains of the fabricated perovskite thin films

Table S3. Elemental compositional ratio of the fabricated $((\text{PEA})_2\text{PbI}_4)_{0.02}(\text{CsPbIBr}_2)_{0.98}$ perovskite thin films from the EDX analyses.

Element	Atomic percentage (%)
Cs	20.91
Pb	16.68
I	19.04
Br	35.06
N	2.40
O	5.91

Table S4. XPS FWHM of the elements present in the fabricated perovskite thin films

Elements	FWHM for X=0 (eV)	FWHM for X=0.02 (eV)
Cs 3d	2.57	1.67
Pb 4f	2.45	2.39
I 3d	2.53	1.64
Br 3d	2.74	1.74
C 1s	2.67	1.6

Table S5. Calculated Urbach energy from the fabricated perovskite thin films using the light energy absorption data.

Sample	E _U (m eV)
X=0	48.78
X=0.01	48.54
X=0.02	45.43
X=0.04	45.76
X=0.08	117.64
X=0.1	147.0

Table S6. Hysteresis index calculation from the J-V plot of the fabricated PSCs.

Device	PCE (F)	PCE (R)	HI (%)
W/o	7.09	8.08	12.25
W(X=0.01)	9.35	10.09	7.33
W(X=0.02)	9.58	10.13	5.42
W(X=0.04)	7.93	8.90	10.89
W(X=1)	1.33	1.97	32.48

Table S7. J_{SC} values extracted from J-V, and EQE plot of the fabricated pristine and champion devices.

Device	$J_{SC JV}$ (mA/cm²)	$J_{SC EQE}$ (mA/cm²)
X=0	13.12	12.70
X=0.02	14.36	14.07

Table S8. Statistical analyses of the photovoltaic parameters of the fabricated pristine, and champion devices.

Device	J_{SC} (mA/cm ²)	V_{oc} (V)	FF (%)	PCE (%)
With additive	13.53±0.70	1.12±0.01	0.60±0.01	9.23±0.69 10.13
Without additive	12.40±1.08	1.04±0.04	0.55±0.01	7.19±0.95 8.08

- The bolded digits correspond to the maximum achieved device *PCE* values. The whole analyses were done considering the reverse scanning J-V plot only.

Table S9. Electrochemical impedance spectroscopy (EIS) fitted data using an equivalent circuit model.

Device	Rs (Ω)	Rct (Ω)	Rrec (Ω)	CPEtr (S-sec ⁻ⁿ)	CPErec (S-sec ⁻ⁿ)
X=0	30.7	607	627.1	6.9X10 ⁻⁷	1.4X10 ⁻⁴
X=0.02	22.34	924.4	808.1	5.2X10 ⁻⁷	1.3X10 ⁻⁴

Table S10. Parameters of the different layers of the PSCs for the numerical simulation using SCAPS 1D software.

Parameters	FTO ¹	CsPbIBr ₂ ²	TiO ₂ ³	Spiro-OMeTAD ⁴
<i>d</i> (nm)	200 (experimental)	598 (experimental)	505 (experimental)	115 (experimental)
<i>E_g</i> (eV)	3.5	2.06 (experimental)	3.2	2.9
χ (eV)	4.0	3.7	4.2	2.2
ε_r	9	8	9	3
<i>N_c</i> (cm ⁻³)	2.2X10 ¹⁸	2.0X10 ¹⁸	10 ¹⁸	2.5X10 ¹⁸
<i>N_v</i> (cm ⁻³)	1.8X10 ¹⁹	5.0X10 ¹⁸	10 ¹⁹	1.8X10 ¹⁹
μ_n (cm ² /Vs)	2.0	20	5X10 ⁻²	2.0X10 ⁻⁴
μ_p (cm ² /Vs)	1.0	20	5X10 ⁻²	2.0X10 ⁻⁴
<i>V_e</i> (cm/s)	1.0X10 ⁷	1.0X10 ⁷	10 ⁷	1.0X10 ⁷
<i>V_h</i> (cm/s)	1.0X10 ⁷	1.0X10 ⁷	10 ⁷	1.0X10 ⁷
<i>N_A</i> (cm ⁻³)	0	1.0X10 ¹⁵	0	1.0X10 ²²
<i>N_D</i> (cm ⁻³)	1.0X10 ¹⁹	0	10 ¹⁸	0
<i>N_t</i> (cm ⁻³)	1.0X10 ¹⁴ (experimental)	5.12X10 ¹⁵	10 ¹⁴	1.0X10 ¹⁴
<i>A_a</i> (cm ⁻¹)	Scaps value	10X10 ⁷ (experimental)	Scaps value	Scaps value

■ The N_t for the champion device was also taken experimentally, which is 4.32X10¹⁵ cm⁻³.

- Numerical simulation of the PSCs using SCAPS 1D:

To study a little deeper inside the device physics of our fabricated PSCs, we have studied a numerical simulation of the PSCs using a solar cell capacitance simulator one dimension (SACPS 1D; version 3.3.09) software^{5,6}. The three equations that make up this software are Poisson's equation (1), the electron-hole continuity equation (2), and the energy band-to-voltage (J-V) equation (3). These equations are solved to provide the optical and electrical properties.

$$\frac{\partial}{\partial x} (-\varepsilon(x) \frac{\partial V}{\partial x}) = q[p(x) - n(x) + N_D^+(x) - N_A^-(x) + p_t(x) - n_t(x)] \dots \quad (1)$$

Where, ε , V , q , $p(x)$, $n(x)$, $N_D^+(x)$, $N_A^-(x)$, $p_t(x)$, and $n_t(x)$ denoted the dielectric permittivity, electric potential, electronic charge, free hole concentration, free electron concentration, ionized donor concentration, ionized acceptor concentration, trap density of holes, and trap density of electrons, respectively. The $J_n, J_p, R_n, R_p, G_n, G_p$ are referred to the current density, recombination rate, and generation rate corresponding to the electron and hole, respectively.

In this SCAPS 1D numerical simulation, we have presented a list of the main characteristics of materials used in the fabrication of the PSC. The terms thickness, bandgap, electron affinity, relative dielectric permittivity, effective conduction band density, effective valance band density, electron mobility, hole mobility, electron thermal velocity, hole thermal velocity, shallow acceptor density, shallow donor density, total defect density, and absorption coefficient are represented by the terms d , E_g , χ , ε_r , N_c , N_v , μ_n , μ_p , V_e , V_h , N_A , N_D , N_t , A_a in the Table S12. Except, the thickness of each material, and the absorption coefficient, & the total defect density (N_t) of the perovskite

absorber layer, all properties of the materials used in the numerical simulation are taken from previously reported articles.

References

- (1) Isoe, W. M.; Mageto, M. J.; Maghanga, C. M.; Mwamburi, M. M.; Odari, B. V. Optical Modelling of TCO Based FTO/TiO₂ Multilayer Thin Films and Simulation in Hydrogenated Amorphous Silicon Solar Cell. *Scientific African* **2023**, *20*, e01678.
- (2) Khatoon, S.; Chakraborty, V.; Yadav, S. K.; Diwakar, S.; Singh, J.; Singh, R. B. Simulation Study of CsPbIxBr_{1-x} and MAPbI₃ Heterojunction Solar Cell Using SCAPS-1D. *Solar Energy* **2023**, *254*, 137–157.
- (3) Sawicka-Chudy, P.; Starowicz, Z.; Wisz, G.; Yavorskyi, R.; Zapukhlyak, Z.; Bester, M.; Głowa, Ł.; Sibiński, M.; Cholewa, M. Simulation of TiO₂/CuO Solar Cells with SCAPS-1D Software. *Materials Research Express* **2019**, *6* (8), 085918.
- (4) Das, T.; Guchhait, A. Effect of Doping in ZnO Nanorod ETL Based Perovskite Solar Cells: Numerical Modeling to Experimental Verification. *Materials Today: Proceedings* **2024**. <https://doi.org/10.1016/j.matpr.2024.01.039>.
- (5) Burgelman, M.; Nollet, P.; Degrave, S. Modelling Polycrystalline Semiconductor Solar Cells. *Thin Solid Films* **2000**, *361–362*, 527–532.
- (6) Das, T.; Rana, N. K.; Guchhait, A. Structural Optimization of Inverted CsPbI₂Br Perovskite Solar Cells for Enhanced Performance via SCAPS-1D Simulation. *Physica Scripta* **2023**, *98* (7), 075928.